JOURNAL OF CATALYSIS **161,** 819–828 (1996)
ARTICLE NO. 0245

NaY-Supported Molybdenum Sulfide Catalysts

I. Catalysts Prepared via Impregnation with Ammonium Heptamolybdate

W. J. J. Welters, G. Vorbeck, H. W. Zandbergen,* L. J. M. van de Ven, E. M. van Oers, J. W. de Haan, V. H. J. de Beer, and R. A. van Santen

*Schuit Institute of Catalysis, Eindhoven University of Technology, P.O. Box 513, 5600 MB Eindhoven, The Netherlands; and *Center for High Resolution Electron Microscopy, Delft University of Technology, Rotterdamseweg 137, 2628 AL Delft, The Netherlands*

Received July 5, 1994; revised February 2, 1996; accepted March 22, 1996

NaY-supported molybdenum sulfide catalysts with increasing Mo loading have been prepared by impregnation with ammonium heptamolybdate and characterized by means of thiophene hydrodesulfurization (HDS), overall sulfur analysis, temperature programmed sulfidation, N_2 adsorption, Xe adsorption, ^{129}Xe-NMR, and high resolution electron microscopy. After impregnation nearly all Mo is located on the exterior of the zeolite particles. During calcination in air part of the Mo is redistributed, resulting in a higher amount of Mo being located in the zeolite supercages. For the sulfided catalysts an amount of Mo comparable to that after calcination is present in the supercages. At the highest Mo loadings the catalysts are incompletely sulfided, due to the presence of large "bulk-like" molybdenum oxide particles on the outside of the zeolite particles. The amount of Mo present in the supercages, as well as the thiophene HDS activity of the sulfided catalysts, increases with increasing Mo loading. The small Mo sulfide particles in the supercages contribute strongly to the thiophene HDS activity. © 1996 Academic Press, Inc.

INTRODUCTION

Incorporation of transition metal sulfides into acidic zeolites leads to bifunctional catalysts combining hydrogenation and cracking properties. The catalytic properties of such bifunctional catalysts are strongly influenced by the location (inside or outside the zeolite pores) and dispersion of the metal sulfide phase. In commercial hydrocracking catalysts, Ni-Mo or Ni-W phases are usually present as the hydrogenating component (1). In order to understand the catalytic properties of these bimetallic catalysts a thorough characterization and understanding of their monometallic counterparts is first needed. Therefore, in recent years fundamental research directed to the application of zeolite materials as supports for molybdenum compounds (2–19) has increased. However, only a few of these studies deal with the characterization of molybdenum-loaded zeolites in the sulfided state (14–19).

López Agudo *et al.* (12) studied catalysts prepared via impregnation with ammonium heptamolybdate (AHM) and found that the Y zeolite was losing its crystallinity and thiophene hydrodesulfurization (HDS) activity with increasing calcination temperature. Impregnation with AHM produces essentially an external surface loading of molybdenum due to the failure of the anionic or neutral complexes to penetrate the zeolite cavities in the presence of water. However, thermal decomposition of these species under constant low water vapor pressure produces a redispersion of the molybdenum due to solid state ion exchange of $MoO_2(OH)_2$ within the zeolite pores (7, 12). Nickel and molybdenum sulfides loaded into Y zeolites were characterized with various techniques by Leglise *et al.* (14) and Ezzamarty *et al.* (15). It was claimed that, in most cases, the sulfidation of the transition metals is incomplete.

Up to now it is not clear what causes the incomplete formation of MoS_2 on zeolite-supported Mo catalysts upon sulfidation (14, 15, 19). Possibly, a strong interaction between the Mo species and the zeolite support exists (9, 12) which hampers sulfidation, or hardly sulfidable bulk oxides are formed on the outside of the zeolite crystals (19). Additionally, little information is available about the distribution of the molybdenum phase over the zeolite particles (throughout the zeolite supercages or on the outside). For catalysts prepared via impregnation with AHM, all Mo might at first be located on the outside of the zeolite particles, but during calcination possibly the molybdenum oxide phase is partly redistributed throughout the supercages (7, 12). The location of the Mo species after sulfidation is not yet clear. From XPS measurements on sulfided calcined Mo/HY catalysts it was concluded that the Mo sulfide phase is homogeneously distributed. On the other hand Anderson *et al.* (19) observed (also by means of XPS) agglomeration of Mo species at the surface of the zeolite.

Although in industrial hydrocracking catalysts stabilized Y zeolites are most commonly used (1), in the present study the parent NaY zeolite has been used as a support for the

0021-9517/96 $18.00
Copyright © 1996 by Academic Press, Inc.
All rights of reproduction in any form reserved.

model catalysts. This has been done to avoid side effects on the catalytic activity and molybdenum distribution caused by the presence of extra-framework alumina or voids and defects in the lattice of the stabilized Y zeolite which may also hamper the structure analysis (i.e., via ^{129}Xe-NMR) of the catalysts. Emphasis is put on the sulfidation behavior of NaY-supported Mo catalysts prepared by impregnation with AHM and the distribution of the molybdenum phase over the zeolite particles is extensively studied. The sulfidation behavior is studied by temperature programmed sulfidation (TPS) and overall sulfur analysis, while the distribution of the molybdenum phase is characterized by N_2 adsorption, Xe adsorption, and ^{129}Xe-NMR and high resolution electron microscopy (HREM), combined with energy dispersive X-ray (EDX) analysis. The majority of these techniques have not been used so far to study (sulfided) Mo/NaY. Atmospheric thiophene HDS is used as the test reaction to compare catalytic activities.

EXPERIMENTAL

Catalyst Preparation

A series of catalysts containing different amounts of molybdenum have been prepared by pore volume impregnation of a NaY support ($Na_{54}(AlO_2)_{54}(SiO_2)_{136} \cdot 250H_2O$, PQ CBV-100) with aqueous $(NH_4)_6Mo_7O_{24} \cdot 4H_2O$ solutions of appropriate concentration. After impregnation the samples are dried overnight at 383 K in air followed by pelletizing, grinding, and sieving to obtain a fraction of 0.125–0.425 mm. A portion of the zeolite samples is subsequently calcined (6 K min^{-1} to 673 K, 2 h at 673 K). All samples are stored in a desiccator over a saturated $CaCl_2$ solution. The catalysts are designated Mo(x)/NaY with x representing the weight percentage Mo (calculated on the basis of the water-free zeolite). XRD analysis showed no significant breakdown of the zeolite structure after impregnation, drying, and calcination.

Catalytic Activity

Thiophene HDS activity is measured in a microflow reactor under standard conditions (673 K, 1 atm, 4.0% thiophene in H_2, 50 std cm^3 min^{-1}). Calcined catalyst samples of 0.25 g are sulfided *in situ* using a mixture of 10% H_2S in H_2 (60 std cm^3 min^{-1}, 6 K min^{-1} from 293 K to 673 K, 2 h at 673 K). After sulfidation the H_2S/H_2 flow is switched to thiophene/H_2. Reaction products are analyzed by on-line G.C. analysis. The first sample is taken after 2-min reaction time and the subsequent ones at intervals of 35 min.

Due to the presence of a few acid sites some polymerization of unsaturated products and cracking of butenes and polymerized products takes place, resulting in some coke formation and a few additional products besides the usual butenes and n-butane. Therefore, thiophene converted to any of the reaction products, including coke, is taken into account for the calculation of the reaction rate constant (k_{HDS}), assuming first-order kinetics in thiophene (20).

TPS and Overall Sulfur Analysis

The total sulfur content is determined by dissolving a sulfided sample in aqua regia while carefully heating the mixture. During this process all molybdenum species are dissolved and the molybdenum sulfide is completely converted into sulphate. The amount of sulphate is determined by titration with barium perchlorate, while the molybdenum content of the solution is analyzed by AAS. Before analysis the catalyst is sulfided using the same procedure as for the HDS activity tests. The sulfided sample is flushed with dry He at 673 K for 1 h to remove adsorbed H_2S and cooled under He. At room temperature the sample is exposed to air and the analysis procedure is started.

The sulfidation process is studied in more detail by temperature programmed sulfidation (TPS). A detailed description of this technique has been given elsewhere (21, 22). A sulfiding gas mixture of 3.3% H_2S, 28.1% H_2, and 68.6% Ar (40 std cm^3 min^{-1}) is passed over a catalyst sample loaded in a quartz tube which is placed in an oven. The H_2S concentration in the reactor outlet is measured by a UV detector (at 195 nm). After H_2O and H_2S are trapped using molecular sieves and ZnO, respectively, the gas flow is led through a thermal conductivity detector where changes in the H_2 concentration are monitored. The measurements are carried out as follows. The reactor is flushed with argon to remove air, followed by sulfidation at room temperature for 10 min. Then, the reactor temperature is raised at 6 K min^{-1} up to 673 K, kept constant for 1 h, and further increased at 10 K min^{-1} up to 1273 K.

Xe Adsorption, ^{129}Xe-NMR, and N_2 Adsorption

To study the presence of molybdenum species inside the zeolite pore system ^{129}Xe-NMR experiments are carried out in combination with Xe adsorption measurements. The principle (23, 24), experimental details (25, 26), and quantitative aspects (26) of this technique have been extensively described elsewhere. Three series of samples are measured: (I) the noncalcined samples carefully dried in He prior to Xe adsorption and ^{129}Xe-NMR (1 K min^{-1} to 453 K, 2 h at 453 K); (II) He dried and calcined samples; and (III) sulfided calcined samples (sulfidation: same as for the catalytic activity measurements, followed by flushing with He for 1 h at 673 K and cooling under He). To avoid contact with O_2 and H_2O the samples are transferred into the NMR tubes using a recirculation-type glove box (O_2 and H_2O content lower than 2 ppm). They are evacuated at room temperature to a pressure below 10^{-4} mbar and stored in a volumetric adsorption apparatus. At 303 K Xe is adsorbed at different pressures. The NMR spectra are recorded at

the same temperature on a Bruker MSL 400 spectrometer at 110.7 MHz with pulse excitation (0.5 s pulse delay) on stationary samples. The number of scans varies between 2×10^2 and 10^5.

For the calcined and sulfided samples also the BET surface area and the micropore volume are determined by N_2 adsorption at 77 K using a Carlo Erba Sorptomatic 1900. After sulfidation (see ^{129}Xe-NMR experiments) they are transferred into the sample holder without exposure to O_2 or H_2O.

High Resolution Electron Microscopy

To study the amount of molybdenum phase located at the exterior of the zeolite particles HREM is performed on oxidic and sulfided samples, using a Philips CM 30 ST electron microscope. After grinding, the zeolite particles are suspended in alcohol. A copper grid coated with a micro grid carbon polymer is loaded with a few droplets of this suspension. The Mo distribution throughout the zeolite particles can be studied (integrally or segment-wise) by means of EDX analysis, in combination with HREM.

In order to investigate the Mo sulfide content inside the zeolite cavities, ion milling is applied to make specimens sufficiently thin, such that only the interior of a zeolite crystal remains. For this method about 20 μm thick pellets are pressed and ion milled with 5 keV Ar ions (15° incidence angle and a current of 1 mA) until a hole is formed. Next, 2 keV Ar ions with 10° incidence angle are applied for 30 min to reduce the thickness of the amorphous layer. Since in this way a random cut is made out of the pellet, one has to take into account the possibility that not a slice of the interior of a crystal is obtained, but rather a slice containing also part of the surface.

RESULTS

Catalytic Activity

As can be seen in Fig. 1, it is only up to 1 h run time that the NaY support shows any HDS activity. The activities of the sulfided Mo/NaY samples show much higher than that of the NaY support. Except for Mo(10)/NaY, which shows a weak deactivation, all catalysts have stable catalytic activity, indicating that there is no substantial sintering of the metal sulfide phase and/or coke formation during the 2 h test run. The products mainly consist of butenes. The product selectivity for n-butane is always less than 10% and slightly increases as the Mo content becomes higher. Besides these C_4 products also some products of cracking and polymerization are observed. In contrast to the NaY-supported nickel sulfide catalysts (27), the amounts of these products are small (the product selectivity for C_4 products is around 90% for all catalysts), indicating an almost complete absence of acid sites. The HDS activity increases with Mo loading, but the increase is not proportional.

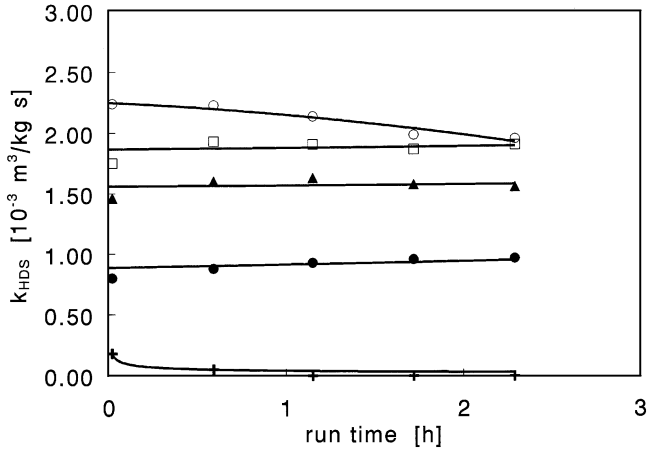

FIG. 1. Thiophene HDS activity as a function of run time for a series of Mo(x)/NaY catalysts differing in Mo loading: +, NaY; ●, 3.5 wt% Mo; ▲, 5.4 wt% Mo; □, 7.8 wt% Mo; ○, 10.0 wt% Mo.

TPS and Overall Sulfur Analysis

The NaY support itself shows no measurable H_2S or H_2 consumption or production, except for a small H_2S and H_2 peak at about 1200 K, which coincides with the collapse of the zeolite framework. Sulfidation of the calcined Mo (5,4)/NaY sample starts already at the isothermal stage at room temperature. Immediately after exposure to H_2S/H_2, some H_2S consumption occurs, accompanied by a color change from white to brownish. After the start of the temperature program some H_2S desorption is observed, followed by H_2S consumption (320–485 K; see Fig. 2). No H_2 consumption is found below 470 K. Around 525 K a strong H_2 consumption occurs, while simultaneously H_2S is produced. The H_2 consumption continues at temperatures above 550 K, but at the same time the H_2S desorption becomes very low. After the isothermal stage at 673 K the H_2S and H_2 consumption is ca. 1.2 H_2S/Mo and 0.9 H_2/Mo, respectively. Clearly, sulfidation has not been completed at 673 K. This can also be concluded from the sulfidation behavior above 673 K. At first, some additional H_2 is consumed, accompanied by H_2S desorption. Above 825 K this is followed by a rather strong H_2S consumption. At 1200 K some H_2 and H_2S desorption takes place, caused by the collapse of the zeolite framework. The total amounts of H_2 and H_2S consumed up to 1273 K are 1.1 H_2/Mo and 2.0 H_2S/Mo, indicating that sulfidation is completed.

For all sulfided (at 673 K) catalysts both the Mo and the S content are analyzed. The results are given in Table 1. From the S/Mo ratios it can be concluded that only the catalyst containing 3.5 wt% Mo is fully sulfided. For the other catalysts the degree of sulfidation decreases as the Mo content increases.

Compared with the TPS experiment the overall sulfur analysis shows a higher degree of sulfidation for the Mo(5.4)/NaY sample (60% sulfidation vs 90%). This may

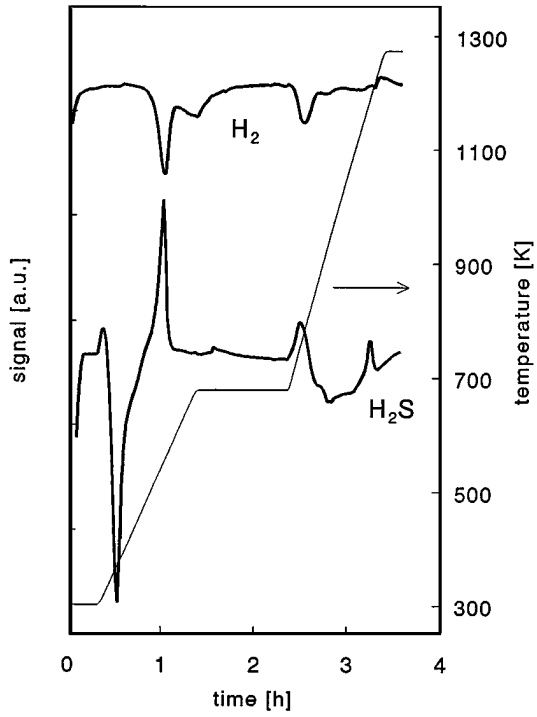

FIG. 2. TPS pattern of a Mo(5.4)/NaY catalyst. A positive peak means production; a negative peak is consumption.

be due to a longer isothermal sulfidation at 673 K (2 h vs 1 h) and/or a higher H_2S partial pressure (10^4 Pa vs 3.3×10^3 Pa) applied for overall sulfur analysis.

N_2 and Xe Adsorption and ^{129}Xe-NMR

It is known that the shapes of the N_2 adsorption isotherms for zeolites are not very informative and classical methods for calculation of the monolayer capacity do not work. Thus, the zeolite surface areas determined by the BET method cannot be considered equal to the true values, even though they may approach them. Also, the micropore volumes derived from these N_2 adsorption measurements give no absolute values for the pore volume of the zeolite, as the packing of the N_2 molecules in the zeolite pores is probably poor. However, the BET method can be used to compare zeolite samples of the same origin (28). The BET surface areas and micropore volumes are listed in Table 2. For the calcined and (slightly more pronounced) for the sulfided Mo(x)/NaY samples the surface area and the micropore volume clearly decrease monotonously with increasing Mo content.

TABLE 1

Degree of Sulfidation of Mo(x)/NaY as Determined by Overall Sulfur Analysis

Catalyst	S/Mo ratio
Mo(3.5)/NaY	2.2
Mo(5.4)/NaY	1.8
Mo(7.8)/NaY	1.7
Mo(10.4)/NaY	1.3

TABLE 2

BET Surface Area and Micropore Volume of the Calcined and Sulfided Mo(x)/NaY Catalysts

	Calcined samples		Sulfided samples	
Catalyst	Surface area [m^2/g NaY]	Micropore vol. [cm^3/g]	Surface area [m^2/g NaY]	Micropore vol. [cm^3/g]
NaY	852	0.34	846	0.33
Mo(3.5)/NaY	813	0.30	775	0.29
Mo(5.4)/NaY	762	0.28	671	0.25
Mo(7.8)/NaY	724	0.27	624	0.24
Mo(10.4)/NaY	673	0.26	613	0.23

Figures 3a, b, and c show the Xe adsorption isotherms for the noncalcined, calcined, and sulfided samples. The amounts of adsorbed Xe exhibit a linear dependence on the Xe pressure for almost all samples. Only for calcined Mo(10)/NaY is the isotherm slightly curved. The noncalcined samples show a very small decrease of the adsorption capacity with increasing Mo loading, indicating that only a very small fraction of the Mo has entered the zeolite pores after impregnation. Upon calcination the decrease of the adsorption capacity with increasing Mo loading is much stronger. Apparently, the amount of Mo in the zeolite supercages has increased after calcination. Except for Mo(3.5)/NaY sulfidation results in a small additional decrease of the adsorption capacity.

As can be seen in Figs. 4a, b, and c, all samples show a linear increase of the ^{129}Xe NMR chemical shift with the increasing amount of Xe adsorbed. The chemical shift of the ^{129}Xe NMR signal, extrapolated to zero xenon density (zero Xe adsorbed), also increases with increasing metal loading. For all metal loadings the highest extrapolated chemical shift is found for the sulfided samples.

HREM

Both a calcined oxidic and a sulfided Mo(10.0)/NaY sample have been examined by HREM. In the oxidic sample some zeolite particles with high amounts of Mo are present (measured by EDX), while on others the concentration is much lower. Occasionally, some needle-shaped molybdenum oxide particles are observed on the outside of the zeolite crystals. Some amorphous parts consist mainly of Na, Mo, and O, indicating that Na_2MoO_4 may have been formed during impregnation. From EDX experiments a relative amount of Mo located inside the zeolite cavities can be estimated. For this estimation, EDX is carried out on a sample area consisting of a fairly thick zeolite crystal, showing clearly the zeolite lattice, but not showing any

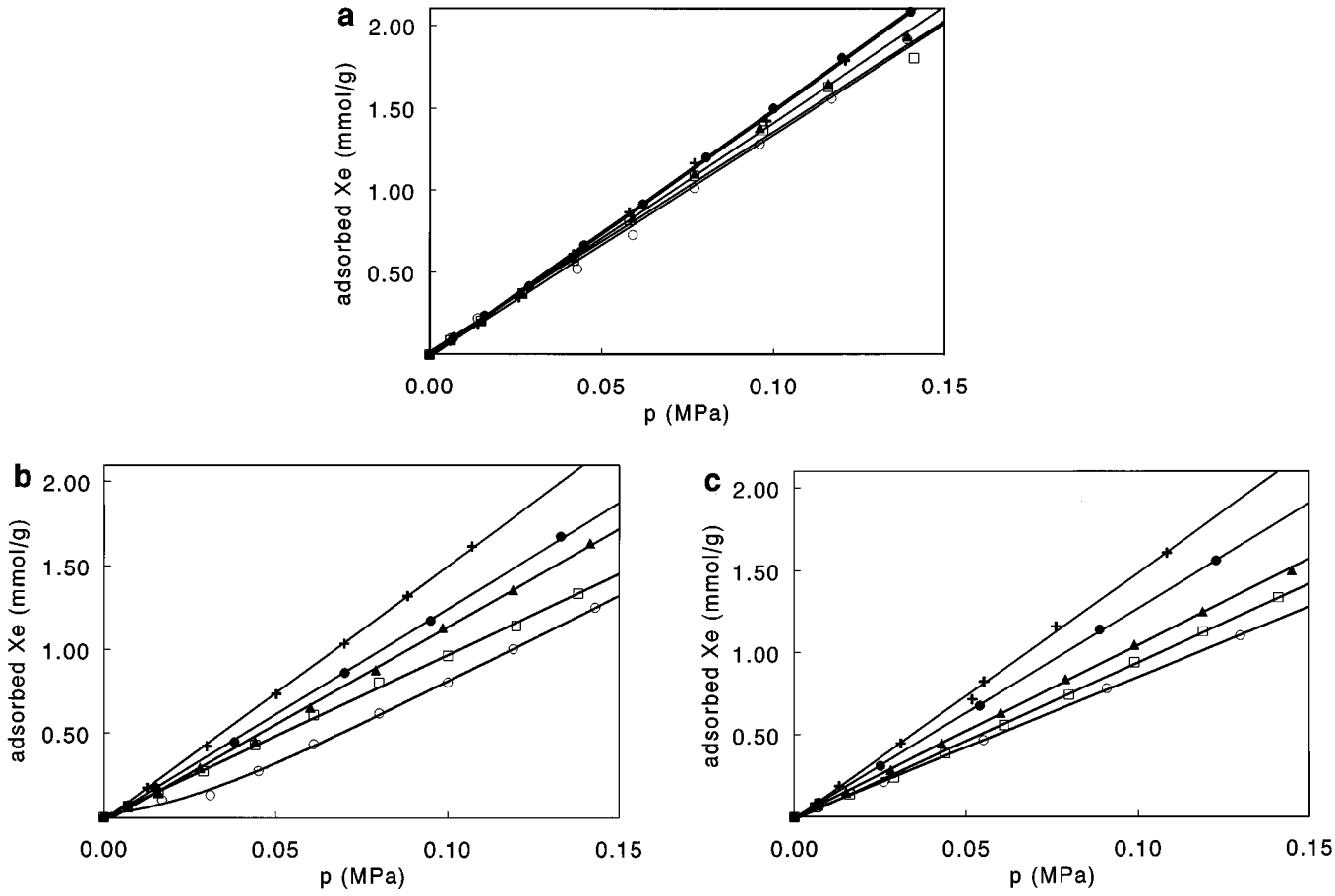

FIG. 3. Xe adsorption isotherms (mmol/g NaY) for different Mo(x)/NaY catalysts: (a) noncalcined samples; (b) calcined samples; (c) sulfided samples. +, NaY; ●, 3.5 wt% Mo; ▲, 5.4 wt% Mo; □, 7.8 wt% Mo; ○, 10.0 wt% Mo.

sign of Mo-containing particles (small "Mo" particles not detectable by HREM might still be present on the surface). Because the surface/volume ratio is small for such an area, the main contribution to the EDX spectrum will originate from the zeolite interior. By comparison of the Mo/Si ratio measured from measurements of several areas composed of many well-structured zeolite and (HREM-detectable) Mo-rich particles it was estimated that at most 25% of the Mo is located inside the zeolite crystals.

From the above results it can be concluded that in the case of oxidic (calcined) Mo(10.0)/NaY both the distribution of Mo over the internal and external zeolite surface and over the various zeolite particles is very inhomogeneous.

After sulfidation, again a very inhomogeneous distribution of the Mo species is found. Large parts of the outer surface are covered with MoS_2 slabs, while other parts contain only a few small MoS_2 slabs (Fig. 5a). Occasionally, some very large amounts of MoS_2 are present on amorphous parts at the outer surface of some zeolite particles (see Fig. 5b). No areas showing MoS_2-free zeolite outer surface are observed in the sulfided Mo(10.0)/NaY samples. Consequently, the Mo concentration inside these particles could not be estimated by EDX. The electron beam always passes a surface region when it enters and leaves the particles, and the Mo in these surface regions will also contribute to the EDX spectrum. In order to determine the Mo concentration inside these zeolite particles, they have to be cut to remove the top and bottom parts in such way that the electron beam only interacts with the interior part. This is done by ion milling. By comparison of the overall EDX spectrum of several zeolite particles with those taken on both the edges and the centre of the zeolite slices prepared by ion milling the relative amount of Mo located in the zeolite pores could be estimated at approximately 20%. From these experiments it can also be concluded that both Mo and S are present inside the zeolite, indicating that the Mo species present in the zeolite cavities are sulfided.

DISCUSSION

Catalytic Activity

The low thiophene conversion observed for the NaY support can be explained by the presence of some acidic

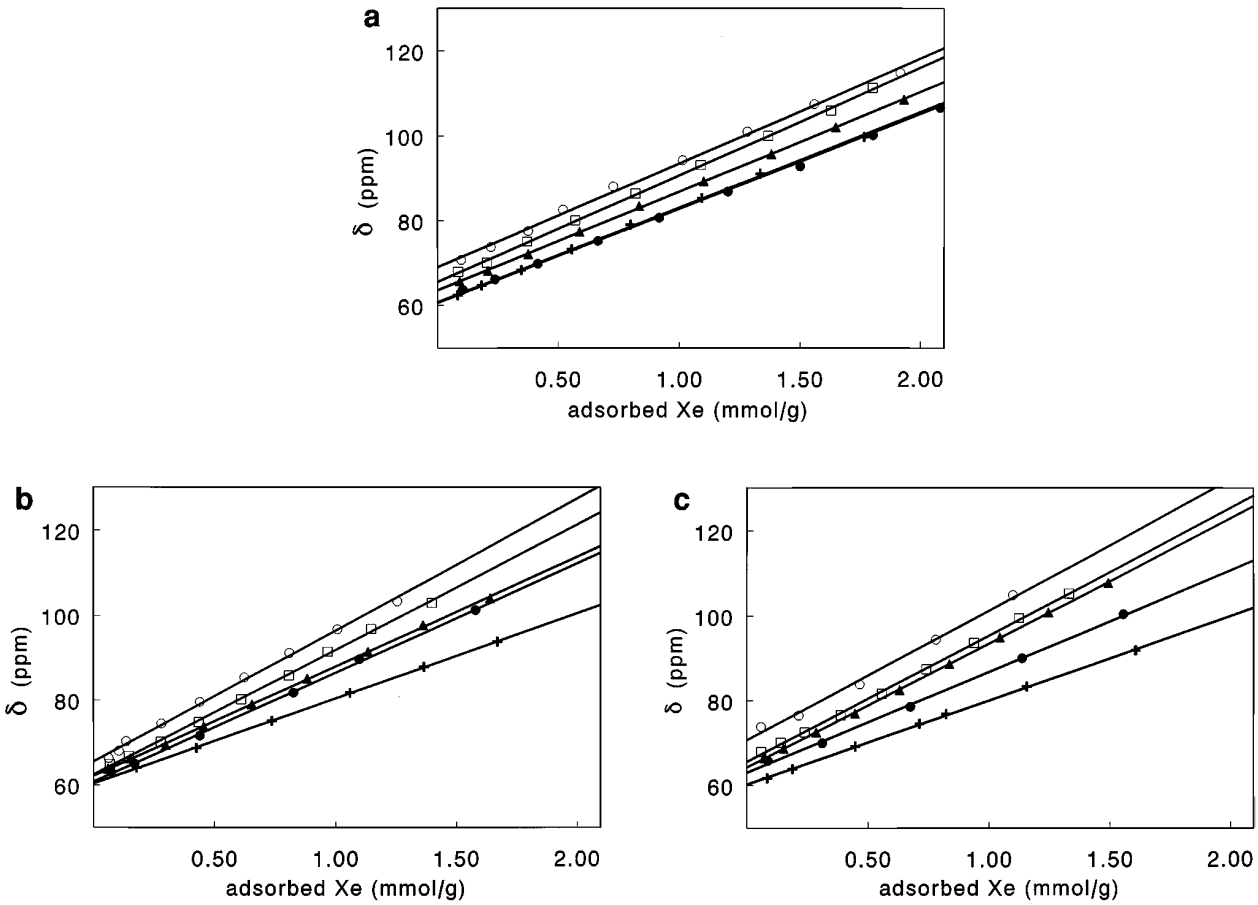

FIG. 4. The ^{129}Xe chemical shift as a function of the adsorption (mmol/g NaY) for different Mo(x)/NaY catalysts: (a) noncalcined samples; (b) calcined samples; (c) sulfided samples. +, NaY; ●, 3.5 wt% Mo; ▲, 5.4 wt% Mo; □, 7.8 wt% Mo; ○, 10.0 wt% Mo.

OH-sites formed by interaction between H_2S and Na ions (30) during sulfidation. Acidic zeolites have a considerable thiophene HDS activity in the absence of a metal sulfide phase (18, 29).

The formation of small amounts of cracking and polymerization products in the case of sulfided Mo(x)/NaY catalysts indicates that a few acid sites are also present on these catalysts. It is plausible that these sites result from some exchange of the Na^+ ions in NaY by NH_4^+ ions in the $(NH_4)_6Mo_7O_{24}$ solution during impregnation. After drying and decomposition of the AHM, Na_2MoO_4 particles are formed, both in the interior and on the exterior of the zeolite crystals. In the latter case their presence is found by combined HREM–EDX analysis.

The increase in activity with increasing molybdenum content is probably caused by an enlargement of the Mo sulfide surface area. The activity (measured after 2 h run time) levels off at higher metal loadings, which indicates that the overall Mo sulfide dispersion decreases at higher Mo loading. For carbon-supported Mo sulfide catalysts a similar behavior as a function of the Mo loading was observed (31). Although they have a higher activity at short run times they deactivate, whereas their Mo/NaY-supported counterparts are remarkably stable and as a result both types of catalysts show similar thiophene HDS activities after 2 h run time. Compared with Mo(x)/Al_2O_3 catalysts (31) the Mo/NaY catalysts clearly show higher HDS activities, both initially and after 2 h reaction. This is in line with the results obtained for zeolite Y supported Ni and Co sulfide catalysts (32). Just like carbon, the NaY zeolite seems to function as an inert support for metal sulfides.

Sulfidation Behavior

The sulfidation picture emerging from the TPS results obtained for Mo(5.4)/NaY is approximately the same as that described by others for Mo/Al_2O_3 (22, 23), Mo/carbon (33, 34), and Mo/SiO_2 (33, 35, 36) catalysts: (i) Already at room temperature some sulfidation is observed (some irreversible H_2S uptake and a color change from white to brownish). (ii) At increasing temperatures the sulfidation proceeds via O–S exchange on Mo^{6+} (strong H_2S and zero

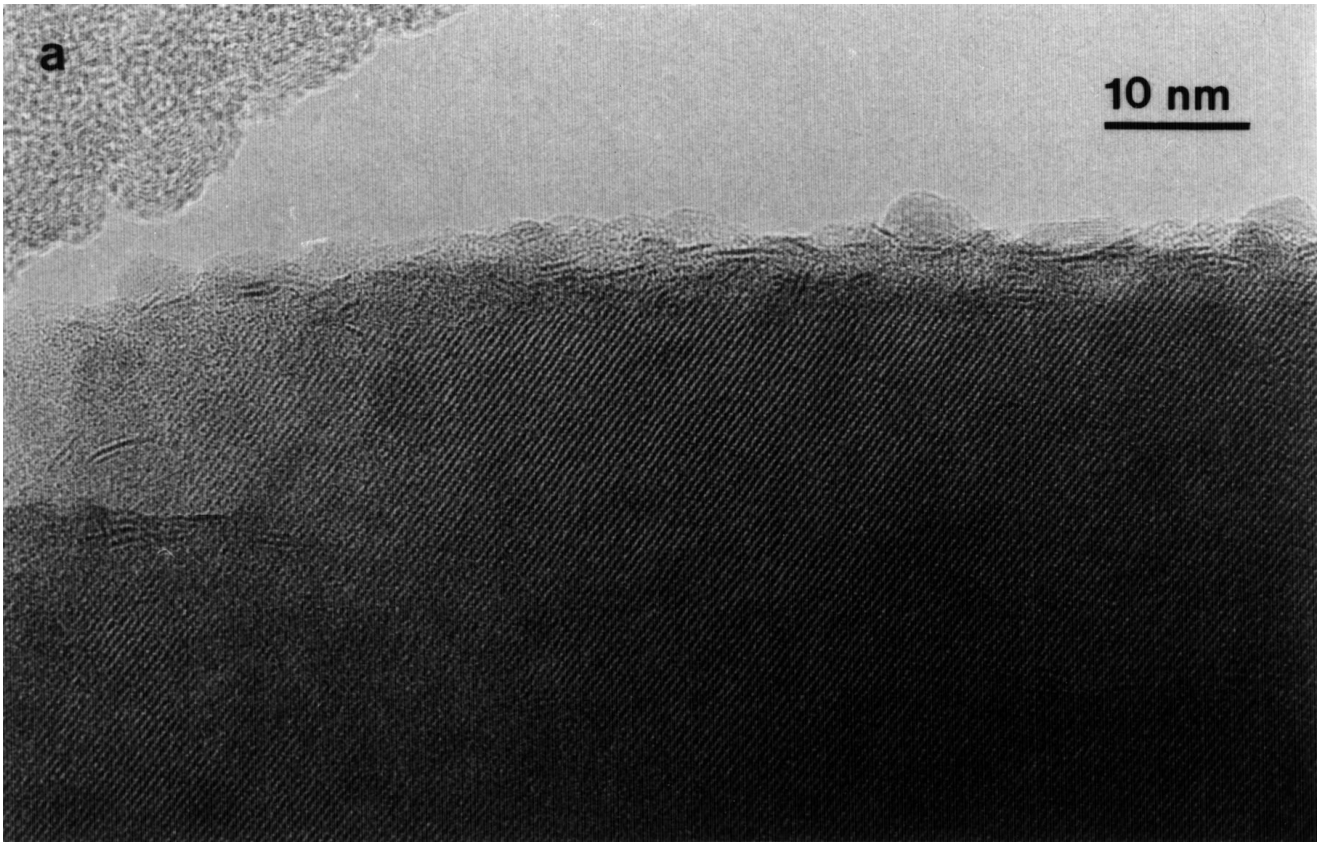

FIG. 5. HREM pictures of a sulfided Mo(10.0)/NaY catalyst: (a) shows an area containing relatively little MoS_2 on the external zeolite surface. The amorphous area in the left upper corner is the carbon film of the supporting grid. The zeolite surface contains also some particles which are probably not MoS_2, some of which are amorphous. (b) shows large MoS_2 particles on the zeolite surface. Due to strong bending of these particles the dominant 002 fringes can only be seen in parts of the MoS_2 particles.

H_2 consumption). (iii) Finally, reduction of Mo^{6+} via Mo–S bond breaking takes place (strong H_2 consumption and H_2S production). However, typically for the Mo(5.4)NaY sample, above 550 K some further reduction of Mo^{6+} occurs without concomitant H_2S production (Mo–S bond breaking). In addition, unlike for Al_2O_3-, carbon-, and SiO_2-supported catalysts a relatively large part of the Mo species on the NaY zeolite has not been sulfided (S/Mo = 1.2) at 673 K which is the maximum temperature in the sulfidation procedure applied prior to the activity tests. At the same time, the H_2 consumption per Mo atom is 0.9, which means that a considerably larger part of the Mo (VI) has been reduced to Mo (IV) at this temperature. Based on the findings by Arnoldy *et al.* (22) the above TPS results can be ascribed to the presence of large bulk-like MoO_3 particles which are more readily reduced than sulfided.

This is in accordance with the HREM–EDX results showing that in the oxidic state, the size of the molybdenum oxide particles present on the external zeolite surface ranges from small to very large. When the isothermal sulfidation at 673 K is finished, the small Mo oxide particles are quantitatively converted into MoS_2, whereas the large ones are converted into MoO_2 (core part) and MoS_2 (outer part) and they are only fully sulfided when higher temperatures are reached, as can be seen in Fig. 2.

At present we have no explanation for the small H_2S production (about 0.1 mol H_2S per mol Mo) accompanied by an equimolar H_2 consumption observed in the TPS pattern around 775 K. This phenomenon cannot be caused by the reduction of elemental sulfur, MoS_3, or oxy-sulfide species since these species should have been reduced already at far lower temperatures (around 525 K) (22). At 1200 K, after the collapse of the zeolite framework, all Mo is converted into MoS_2.

The decreasing degree of sulfidation at increasing Mo content shown in Table 1 confirms the TPS finding that the incomplete sulfidation is linked with the presence of large Mo oxide particles and not with the presence of very small Mo oxide particles in the NaY supercages. A higher Mo loading will result in more and larger Mo oxide particles, and consequently the degree of sulfidation will be lower.

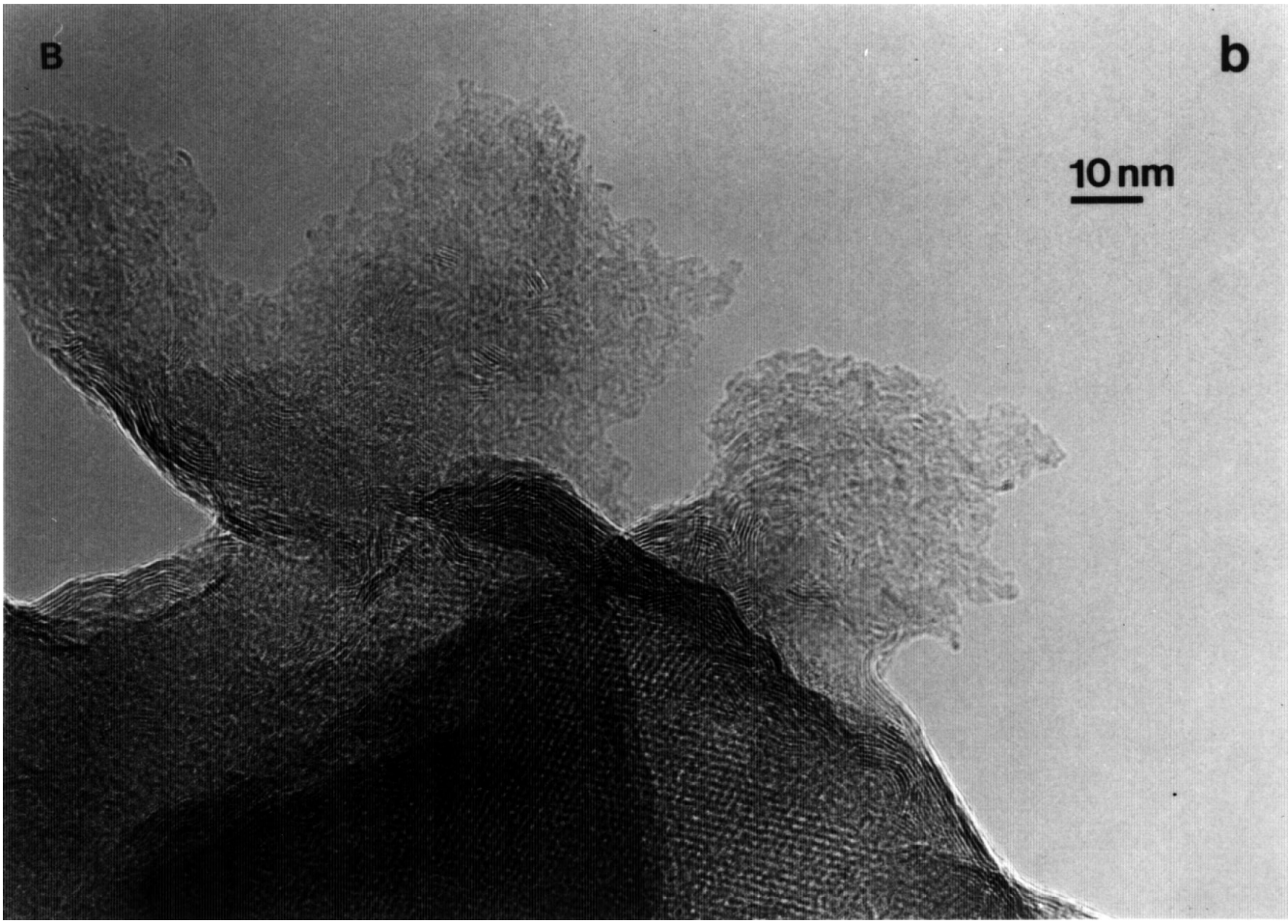

FIG. 5—*Continued*

Also the presence of Na_2MoO_4 (as observed with HREM–EDX) may hamper the sulfidation of Mo at 673 K. In Fig. 5b large particles consisting of MoS_2 located on the outside of a zeolite crystal can be seen. Additionally, some amorphous Mo-containing particles covered by MoS_2 can be seen at the surface. Possibly, these are incompletely sulfided Mo oxide particles. The low degree of sulfidation is in agreement with the results of Leglise *et al.* (14) and Anderson *et al.* (19), who also found an incomplete sulfidation for impregnated stabilized Y-supported samples containing between 4 and 9 wt% Mo.

On the Mo(3.5)/NaY catalyst, even, a slight excess of sulfur is present, compared to the formation of MoS_2. This can be due to the inaccuracy of the analysis method, or perhaps to some elemental S formation during sulfidation. However, as discussed above, all elemental S should have been reduced after sulfidation at 673 K. The reason for the presence of excess S is not clear yet. After sulfidation of pure NaY no sulfur is found, indicating that the excess sulfur is not caused by the zeolite support. It can not be excluded that, also, the other Mo/NaY catalysts contain some excess sulfur, which makes an exact determination of the degree of sulfidation rather difficult.

Distribution of the Mo Species

From the decrease of BET surface areas and micropore volumes with increasing Mo content (Table 2) it can be concluded that both the oxidic calcined and the sulfided samples contain at least part of the Mo species inside the supercages. For all samples the decrease in surface area is proportional to the decrease in pore volume, which indicates that the loss in pore volume is not caused by partial, but by complete filling of the supercages with Mo species or by pore blocking. The latter possibility is sustained by the following. The decrease in pore volume is much larger than the maximum volume that can be occupied by the Mo phase (MoO_3 or MoS_2). In the case of calcined oxidic Mo(10.0)/NaY the decrease is 0.08 $cm^3\ g^{-1}$, while the molybdenum oxide on this sample has a volume of 0.04 $cm^3\ g^{-1}$, assuming all Mo to be present as MoO_3.

The Xe adsorption isotherms of the noncalcined samples show a small but definite decrease in adsorption capacity

with increasing Mo content (Fig. 3a). Likewise, the chemical shift at infinitely low pressure (extrapolation to zero Xe adsorbed) increases (Fig. 4a). These results indicate that already after drying at least a small part of the Mo phase is deposited in the supercages. As the $Mo_7O_{24}^{6-}$ precursor complex is too large its decomposition products must have entered the supercages, either during impregnation or during drying at 383 K.

On the oxidic calcined samples the decrease in adsorption capacity with increasing Mo content is much larger than for the noncalcined samples, indicating that for the calcined samples a larger amount of Mo species is located in the supercages. At the same time, for most of the calcined sample the chemical shift at zero Xe pressure is lower than for the noncalcined samples, which seems to be in contradiction with the lower adsorption capacity of the latter ones. This may be due to the presence of NH_4^+ ions and decomposition products of the $Mo_7O_{24}^{6-}$ complex in the supercages of noncalcined samples which may result in an increased interaction between the Xe nuclei and the sample and, consequently, in a higher chemical shift. After calcination, a higher amount of Mo is present in the supercages, but the Mo phase shows less interaction with the ^{129}Xe atoms (lower chemical shift).

The results indicate that during calcination at least a part of the MoO_3 is redistributed through the supercages. As the calcination was performed in ambient air which contains some water, the redistribution has probably taken place via the formation of $MoO_2(OH)_2$ as proposed by Fierro *et al.* (7). Due to the low vapor pressure of $MoO_2(OH)_2$ (1.7×10^{-4} N m^{-2} at 600 K (37)) and the short calcination period (2 h at 673 K) the amount of MoO_3 redistributed in this way will be limited, resulting in a relatively small amount of Mo located in the supercages (less than 25%, according to the HREM–EDX experiments). The observation that the slope of the chemical shift versus adsorbed Xe plot (Fig. 4b) increases with increasing Mo loading suggests a growing degree of pore blocking (23) by the molybdenum oxide, which agrees with the BET results.

Sulfidation does not significantly change the amounts of Mo species located in the supercages. The adsorption capacities of the calcined and the sulfided Mo(x)/NaY catalysts are also virtually equal. The chemical shifts of the adsorbed ^{129}Xe are somewhat higher for the sulfided catalysts than for the calcined ones. During sulfidation the Mo oxides in the supercages are converted into Mo sulfide. The sulfided species may occupy somewhat more pore volume, as both the BET results and the ^{129}Xe chemical shift indicate that the remaining pore volume became somewhat smaller after sulfidation. In principle, the increase in the chemical shift may also originate from a stronger interaction between the ^{129}Xe and the Mo species in the supercages after sulfidation. From the higher slope at higher Mo content (Fig. 4c) it can be concluded that, similar to the calcined samples, also for the sulfided samples pore blocking occurs.

The conclusions derived from BET, Xe adsorption, and ^{129}Xe-NMR are confirmed by HREM–EDX. For both the calcined and the sulfided catalysts the distribution of the Mo phase is rather inhomogeneous. Neither the BET results nor the Xe adsorption and ^{129}Xe-NMR experiments can be used to quantify the amount of Mo inside the zeolite pores (26). Both techniques, however, indicate that for calcined and for sulfided samples a certain amount of Mo species is present in the supercages. From the EDX results on the ion-milled sulfided Mo(10.0)/NaY sample it can be estimated that approximately 20% of the total Mo content is present in the zeolite pores. These results are in agreement with those reported by Laniecki and Zmierczak (17) who concluded that MoS_2 in Mo/NaY catalysts prepared by impregnation is mainly located on the outside of the zeolite particles. In contrast herewith, Ezzamarty *et al.* (15) concluded from XPS measurements that for sulfided impregnation type Mo/USY catalysts the Mo phase is well dispersed and mainly present in the zeolite cavities.

HREM shows that most of the zeolite particles are covered with large mono- and multi ($\leq$10)-layer MoS_2 particles. Thus, the dispersion of the MoS_2 located on the outside of the zeolite particles is low. Nevertheless, the Mo/NaY catalysts are rather active for thiophene HDS. This strongly indicates that the HDS activity is primarily caused by the (highly dispersed) very small Mo sulfide particles inside the supercages, rather than by the large Mo sulfide particles at the outer zeolite surface. The low overall degree of sulfidation (Table 1) may not have a strong influence on the HDS activity, since the nonsulfided Mo oxide fraction is covered by MoS_2 and further sulfidation will not substantially increase the MoS_2 surface. Based on the N_2 adsorption and ^{129}Xe NMR results the activity increase with increasing Mo loading can be explained by the enlargement of the active surface due to the growing amount of Mo sulfide present in the supercages. Also in the case of sulfided zeolite Y supported Ni or Co catalysts there are indications that especially the small sulfide clusters in the supercages are very active for thiophene HDS (27, 38).

CONCLUSIONS

NaY-supported Mo sulfide catalysts prepared by impregnation with AHM are active thiophene HDS catalysts. During impregnation very little Mo enters the zeolite supercages. During calcination, however, a certain part of the Mo phase is redistributed to the supercages. No major relocation of the Mo takes place during sulfidation. The Mo oxide species in the supercages are most probably fully sulfided, while the Mo phase on the exterior is only partly sulfided. This is caused by the presence of large molybdenum oxide particles of which only the outer layers are

converted into MoS_2, while the core remains unsulfided. The small Mo sulfide particles in the zeolite pores are the main contributors to the thiophene HDS activity of these catalysts. Therefore, further improvement of the catalytic properties may be possible by developing preparation methods resulting in a more selective formation of Mo sulfide inside the supercages.

ACKNOWLEDGMENTS

These investigations were supported by the Netherlands Foundation for Chemical Research (SON) with financial aid from the Netherlands Technology Foundation. The authors thank Professor Dr. J. A. R. van Veen for very stimulating and helpful discussions. Thanks are also due to Mrs. Elemans-Mehring, Mr. J. P. Janssens, and Mr. C. D. de Haan for assistance with the AAS, TPS, and HREM measurements, respectively.

REFERENCES

1. Ward, J. W., *Stud. Surf. Sci. Catal.* **16**, 587 (1983).
2. Dai, P. E., and Lunsford, J. H., *J. Catal.* **64**, 173 (1980).
3. Abdo, S., and Howe, R. F., *J. Phys. Chem.* **87**, 1713 (1983).
4. Cid, R., Gil-Llambias, F. J., Fierro, J. L. G., López Agudo, A., and Villasenor, J., *J. Catal.* **89**, 478 (1984).
5. Komatsu, T., Namba, S., Yashima, T., Domen, K., and Onishi, T., *J. Mol. Catal.* **33**, 345 (1985).
6. Johns, J. R., and Howe, R. F., *Zeolites* **5**, 251 (1985).
7. Fierro, J. L. G., Conesa, J. C., and López Agudo, A., *J. Catal.* **108**, 334 (1987).
8. Okamoto, Y., Meazawa, A., Kane, H., Mitsushima, I., and Imanaka, T., *J. Chem. Soc. Farad. Trans. I* **84**, 851 (1988).
9. Corma, A., Vazquez, M. I., Bianconi, A., Clozza, A., García, J., Pallota, O., and Cruz, J. M., *Zeolites* **8**, 464 (1988).
10. Kováchevá, P., Davidová, N., and Nováková, J., *Zeolites* **11**, 54 (1991).
11. Anderson, J. A., Pawelec, B., and Fierro, J. L. G., *Appl. Catal.* **99**, 37 (1993).
12. López Agudo, A., Cid, R., Orellana, F., and Fierro, J. L. G., *Polyhedron* **5**, 187 (1986).
13. Cid, R., Orellana, F., and López Agudo, A., *Appl. Catal.* **32**, 327 (1987).
14. Leglise, J., Janin, A., Lavalley, J. C., and Cornet, D., *J. Catal.* **114**, 388 (1988).
15. Ezzamarty, A., Catherine, E., Cornet, D., Hemidy, J. F., Janin, A., Lavalley, J. C., and Leglise, J., *in* "Zeolites: Facts, Figures, Future" (P. A. Jacobs and R. A. van Santen, Eds.), p. 1025. Elsevier, Amsterdam, 1989.
16. Okamoto, Y., Maezawa, A., Kane, H., and Imanaka, T., *J. Mol. Catal.* **52**, 337 (1989).
17. Laniecki, M., and Zmierczak, W., *Zeolites* **11**, 18 (1991).
18. López Agudo, A., Benitez, A., Fierro, J. L. G., Palacios, J. M., Neira, J., and Cid, R., *J. Chem. Soc. Farad. Trans.* **88**, 385 (1992).
19. Anderson, J. A., Pawelec, B., Fierro, J. L. G., Arias, P. L., Duque, F., and Cambra, J. F., *Appl. Catal.* **99**, 55 (1993).
20. Duchet, J. C., van Oers, E. M., de Beer, V. H. J., and Prins, R., *J. Catal.* **80**, 386 (1983).
21. Scheffer, B., Dekker, N. J. J., Mangnus, P. J., and Moulijn, J. A., *J. Catal.* **121**, 31 (1990).
22. Arnoldy, P., van den Heykant, J. A. M., de Bok, G. D., and Moulijn, J. A., *J. Catal.* **92**, 35 (1985).
23. Fraissard, J., and Ito, T., *Zeolites* **8**, 350 (1988).
24. Ito, T., and Fraissard, J., *J. Chem. Phys.* **76**, 5225 (1982).
25. Korányi, T. I., van de Ven, L. J. M., Welters, W. J. J., de Haan, J. W., de Beer, V. H. J., and van Santen, R. A., *Catal. Lett.* **17**, 105 (1993).
26. Korányi, T. I., van de Ven, L. J. M., Welters, W. J. J., de Haan, J. W., de Beer, V. H. J. , and van Santen, R. A., *Coll. Surf. A: Physicochem. Eng. Aspects* **72**, 143 (1993).
27. Welters, W. J. J., Vorbeck, G., Zandbergen, H. W., de Haan, J. W., de Beer, V. H. J., and van Santen, R. A., *J. Catal.* **150**, 155 (1994).
28. Gregg, S. J., and Sing, K. S. W., *in* "Adsorption, Surface Area, and Porosity," Academic Press, London, 1982.
29. Welters, W. J. J., de Beer, V. H. J., and van Santen, R. A., *Appl. Catal. A General* **119**, 253 (1994).
30. Karge, H. G., and Raskó, J., *J. Colloid Interface Sci.* **64**, 534 (1978).
31. Vissers, J. P. R., Bachelier, J., ten Doeschate, H. J. M., Duchet, J. C., de Beer, V. H. J., and Prins, R., Proc. 8th Int. Congr. Catal. (Berlin, 1984), Vol. II, p. 387. Verlag Chemie, Weinheim, 1984.
32. Welters, W. J. J., Korányi, T. I., de Beer, V. H. J., and van Santen, R. A., Proc. 10th Int. Congr. Catal. (Budapest, 1992) (L. Guczi, F. Solymosi, and P. Tétényi, Eds.), p. 1931. Elsevier, Amsterdam, 1993.
33. Scheffer, B., Arnoldy, P., and Moulijn, J. A., *J. Catal.* **112**, 516 (1988).
34. Vissers, J. P. R., Scheffer, B., de Beer, V. H. J., Moulijn, J. A., and Prins, R., *J. Catal.* **105**, 277 (1987).
35. de Jong, A. M., Borg, H. J., van IJzendoorn, L. J., Soudant, V. G. F. M., de Beer, V. H. J., van Veen, J. A. R., and Niemantsverdriet, J. W., *J. Phys. Chem.* **97**, 6477 (1993).
36. de Boer, M., van Dillen, A. J., Koningsberger, D. C., and Geus, J. W., *J. Phys. Chem.* **98**, 7862 (1994).
37. Glemser, O., and Haeseler, R. J., *Z. Anorg. Allgem. Chem.* **316**, 168 (1962).
38. de Bont, P. W., Vissenberg, M. J., Boellaard, E., van Santen, R. A., de Beer, V. H. J., and van der Kraan, A. M., *Bull. Soc. Chim. Belg.* **104**, 205 (1995).